Analysis on Common to Differential Mode Conversion Within Automotive Communication Systems

Carina Austermann, Stephan Frei
On-board Systems Lab
TU Dortmund University
Dortmund, Germany
carina.austermann@tu-dortmund.de

***Abstract*—Communication systems with high data rates like CAN FD and Automotive Ethernet are increasingly used in automobiles. New safety-critical driving assistance functions can be realized with the help of these bus systems, but data transmission has to be very reliable. Road vehicles are a challenging electromagnetic environment because of the high density of electric and electronic devices. Power electronic systems can be very close to communication systems. The typical cable type for automotive communication systems is the unshielded twisted wire pair. Common mode disturbances cannot be reduced by this cable type. Due to unavoidable asymmetry in the communication system electromagnetic coupling can also induce critical differential mode voltages. For this reason, the immunity of communication systems to electromagnetic interferences has to be investigated in detail. In this paper, simulation models are presented and validated by measurements to quantify cable coupling to CAN FD and 100BASE-T1 Automotive Ethernet. Both, common and differential mode voltages caused by cable coupling are investigated. Based on measurements and simulations critical influencing parameters on mode conversion are discussed.**

Keywords—100BASE-T1, CAN FD, EMI, Wire Coupling, Mode Conversion

I. Introduction

Bus systems with higher data rates like CAN FD (Controller Area Network with Flexible Data rate) [1] and 100BASE-T1 Automotive Ethernet ([2], [3]) offer the possibility of integration of new functions in vehicles up to autonomous driving. The needed high reliability of data transmission requires a good immunity to electromagnetic interferences. The automotive wiring harness poses a challenging electromagnetic environment. Due to this, studies of immunity and especially the investigation of possible coupling paths are very important. In vehicles switched power electronic systems can be very critical sources of EMI. In [4] and [5] measurements of coupled voltages into a 100BASE-T1 communication system caused by an inverter of a high voltage motor drive are analyzed. The different coupling paths and CM disturbances in a setup of motor drive and PLC communication are discussed in [6]. Therefore, wire coupling can be seen as critical for communication systems.

In this work, wire coupling between two electrical systems is investigated as presented in Fig. 1. The analyzed setup consists of a point-to-point communication system with two transceivers of CAN FD or 100BASE-T1 Automotive Ethernet and a disturbing system consisting of a voltage source with source resistance, a single wire and a resistive load emulating different sources of EMI. The wire coupling between both systems is the investigated coupling path. The coupling from the disturbance source to the communication system as sink can be generally represented by a transfer function in frequency domain. In the following, the coupling from the voltage in the disturbing circuit to common mode voltage at the terminations of the twisted wire pair (TWP) and the conversion from common to differential mode voltage are considered separately. A detailed simulation based investigation of all influencing parameters is presented.

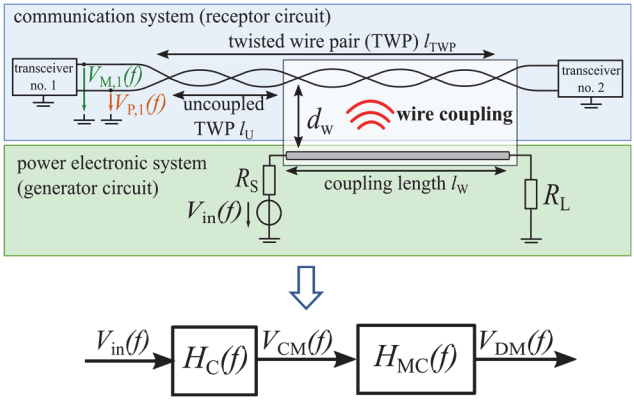

Fig. 1. Investigated setup and relation with examined transfer functions

The paper is structured as follows: In the second chapter, simulation models of communication nodes and coupled wires are presented. Based on the simulation models, the wire coupling leading to common mode disturbance voltage is investigated and the impact of geometry parameters is analyzed (chapter III). Mode conversion is the reason for differential mode disturbing voltages from the common mode disturbances caused by asymmetries in the setup. This is investigated using measurements and simulations in chapter IV.

II. Simulation Models

In this section, the simulation models of communication nodes and coupled wires are presented and validated. The here shown simulations are performed in LTspice.

A. Models of communication nodes

At first, the termination models of the communication network nodes are presented. The equivalent circuits are shown in Fig. 2. In the following investigations, active communication is not analyzed. Therefore, a focus is put on the termination impedances with common mode choke (CMC). The model of CAN FD is shown in Fig. 2 on the right. A standard CAN transceiver model can be found in [7], but without a detailed consideration of termination network including the CMC. The model of the CAN FD termination is parameterized based on the data sheet of evaluation board DSO-8/TSON-8 from Infineon [8]. The simulation model for a 100BASE-T1 termination is also depicted in Fig. 2 (cf. [9]). As reference for the 100BASE-T1 termination model, the

evaluation board DP83TC811EVM of Texas Instruments [10] is used.

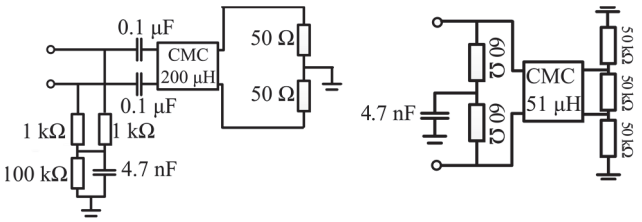

Fig. 2. Simulation models for transceiver termination of 100BASE-T1 (left) and CAN FD (right)

In the modeling, a special focus is put on the CMCs of the terminations. The equivalent circuits of CMCs for both transceiver types are shown in Fig. 3. CAN FD termination includes the CMC type ACT45B-51 from TDK and 100BASE-T1 uses the CMC DLW43MH201XK2L from Murata Electronics.

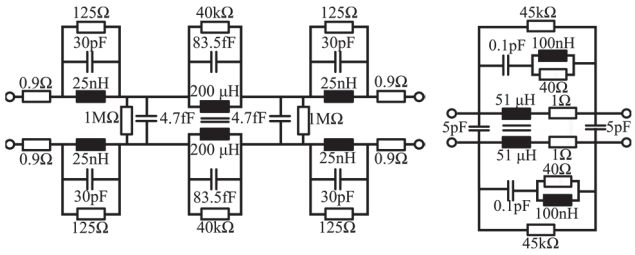

Fig. 3. Equivalent circuit for CMCs used in transceiver termination models for 100BASE-T1 (left) and CAN FD (right)

The validation of the CMC ACT45B-51 model is shown in Fig. 4. The frequency dependent common and differential mode impedances are taken from the data sheet and compared to computed impedances based on S-parameter simulation results using LTspice of the model shown in Fig. 3 (right).

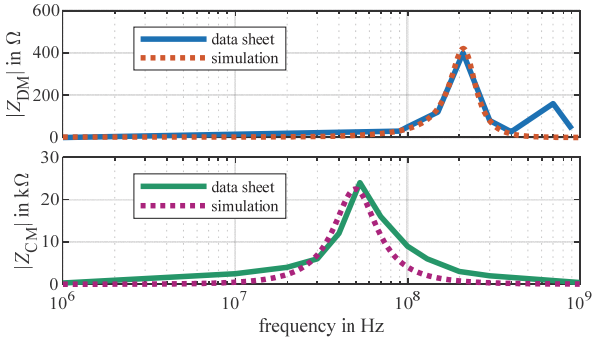

Fig. 4. Validation of the ACT45B-51 model (CAN FD CMC)

The model approach of the CMC in 100BASE-T1 termination is based on [11] but adapted to the used CMC on the evaluation board. The model of DLW43MH201XK2L CMC is parameterized using a 4-port S-parameter measurement with a ZNB8 NWA by Rhode&Schwarz. The differential and common mode impedances from measurement and simulation are depicted in Fig. 5. The simulation results for used CMCs in CAN FD and 100BASE-T1 terminations are close to measurements.

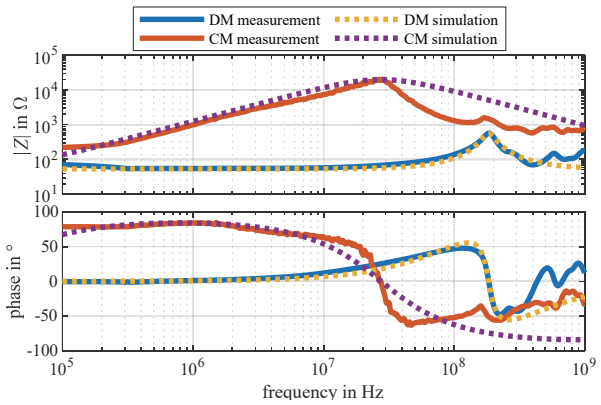

Fig. 5. Validation of DLW43MH201XK2L model (100BASE-T1 CMC)

B. *Models of coupled wires*

The LTspice models of coupled wires are generated using the software tool SACAMOS ([12], [13]). With this software tool the wire coupling between an unshielded twisted wire pair (TWP) and a single wire (SW) can be modeled. Within this tool an ideal TWP without mode conversion is assumed. The used configuration of SW and TWP in parallel over ground plane and required geometry parameters are shown in Fig. 6. The given values of geometry parameters are used in all presented simulations. The wires are placed over a ground plane in the height of 5 cm, if not otherwise specified. The distance between the wires d_W and the length of the coupled wires l_W are varied in the simulations presented in the following.

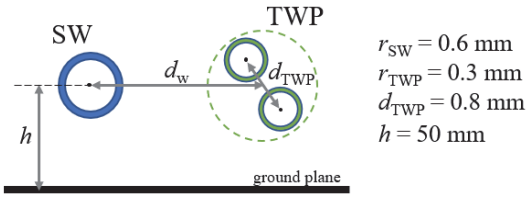

Fig. 6. Wire coupling configuration and required geometry parameters

III. Investigation on Common Mode Disturbances by Wire Coupling

In this chapter, the simulation models are used to quantify the coupling from generator circuit to common mode voltages in the communication system using transfer functions. Different setups are investigated to analyze the impact of important parameters.

A. *Simulation setup to determine common mode coupling*

The models of transceivers, coupled wires and disturbance source circuit are combined as shown in Fig. 7 to build up the investigated setup. The gray marked model represents an uncoupled TWP over ground. This is used in some simulations considering that the coupling does not occur over the entire transmission line between the transceivers (cf. Fig. 1).

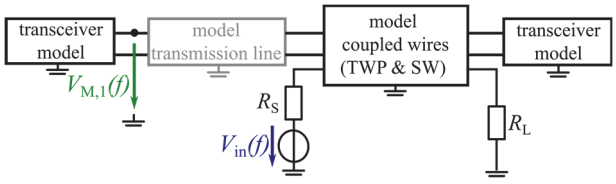

Fig. 7. Simulation setup for computation of transfer function in LTspice

The voltage to ground on the minus wire $V_{M,1}(f)$ at the termination network of communication node is simulated (cf. Fig. 7). Because the simulation setup is completely symmetrical the voltage on one wire equals the common mode voltage and therefore the transfer function can be determined according to (1).

$$H_C(f) = \frac{V_{CM}(f)}{V_{in}(f)} \cong \frac{V_{M,1}(f)}{V_{in}(f)} \quad (1)$$

B. *Verification of wire coupling simulation setup*

The transfer function can be used to calculate CM voltage in time domain within a 100BASE-T1 communication system. The results are compared to measurement data to verify the calculated transfer functions. The used setup is built up according to Fig. 1. The following values are used: $R_L = 50\ \Omega$, $R_S = 0.1\ \Omega$, $l_{TWP} = l_W = 1\ \text{m}$, $d_W = 15\ \text{mm}$. The source of disturbance is a trapezoidal pulse generator with amplitude from 0 to 250 V and a rise time of 10 ns. The determined transfer function computed in a simulation (cf. Fig. 7) is used to calculate the disturbing common mode voltage in time domain. For this purpose, the interfering signal $v_{in}(t)$ is transferred to the frequency domain and multiplied by the transfer function. The common mode voltage is then determined using an Inverse Fast Fourier Transformation (IFFT). The procedure and simulation results are shown in Fig. 8. The comparison in the figure below left of simulation and measurement shows a good conformance.

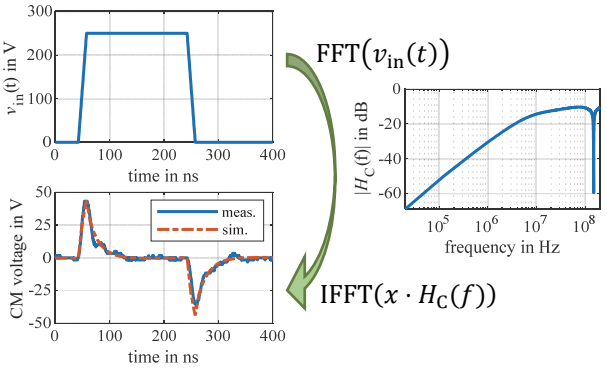

Fig. 8. Verification of transfer function of wire coupling configuration using time domain representation

C. *Simulation results of different wire coupling setups*

The previous verification section III.B has shown the applicability of the simulation setup. In the investigated configuration (cf. Fig. 1) are different parameters, which can influence the coupling and thus the potential disturbance. To find worst-case configurations for both bus systems, the parameters are considered separately. In the first investigations the coupling length is equal to the length of the TWP and the disturbing system cable length. Therefore, in the simulation setup the gray marked transmission line model according to Fig. 7 is not needed. At first, the generator circuit is varied by assuming different load resistors. The resulting transfer functions depending on frequency are shown in Fig. 9. It can be seen, that there are significant differences between the transfer functions for different load resistors. With greater load resistance the current flow through generator circuit is reduced and thus inductive coupling. A special characteristic has the transfer function for $R_L = 1\ \text{k}\Omega$. There is an increase of the transfer function in the frequency range of 50-80 MHz for both communication systems. This can be relevant for 100BASE-T1 transmission because the used symbol duration is 15 ns, which corresponds to 66⅔ MHz. This frequency is marked in red. A sinusoidal interference signal close to this frequency can seriously affect the transmission.

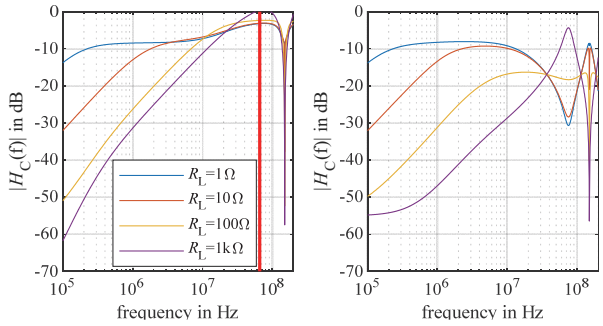

Fig. 9. Transfer function $H_C(f)$ for varying load resistor R_L ($d_W = 2\ \text{mm}$, $l_W = l_{TWP} = 1\ \text{m}$); 100BASE-T1 (left) and CAN FD (right)

An important parameter for the severity of coupling is the distance between the wires. Within a wiring harness the distances between wires can be very small, wires can be even arranged in contact to each other. The simulation results for different distances are shown in Fig. 10. As assumed, the coupling is larger with smaller distances and this applies to all evaluated frequencies. Even for changes in mm range the coupling can vary up to 5 dB.

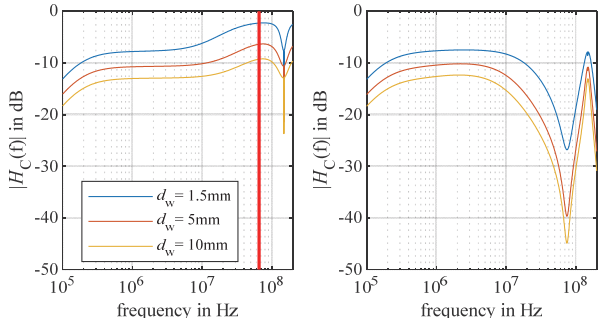

Fig. 10. Transfer function $H_C(f)$ for varying distance between wires d_W ($l_W = l_{TWP} = 1\ \text{m}$, $R_L = 1\ \Omega$); 100BASE-T1 (left) and CAN FD (right)

Another parameter to be analyzed is the coupling length. In this investigation the coupling occurs over the entire length of the TWP ($l_W = l_{TWP}$) between the two communication nodes. The results for three different coupling lengths are depicted in Fig. 11. With different coupling length the resonance within transfer function changes. With increasing coupling length, the resonance frequency decreases.

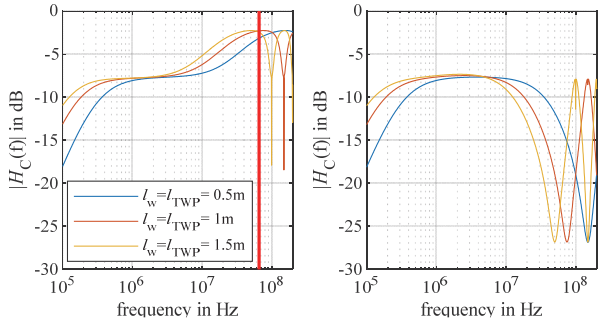

Fig. 11. Transfer function $H_C(f)$ for varying coupling length $l_W = l_{TWP}$ ($d_W = 1.5\ \text{mm}$, $R_L = 1\ \Omega$); 100BASE-T1 (left) and CAN FD (right)

In the previous investigation the height over ground was constant $h = 5\ \text{cm}$. In Fig. 12 the transfer functions for different heights over ground are shown representing the

distance of the chassis to the wiring harness. With an increasing height the coupling increases for all frequencies due to the enlargement of the mutual inductance.

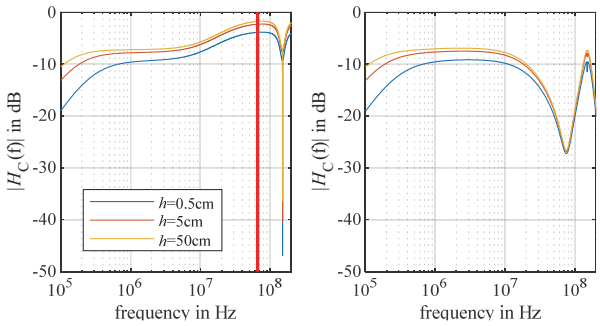

Fig. 12. Transfer function $H_C(f)$ for varying height over ground h ($l_w = l_{TWP} = 1\text{m}$, $d_w = 1.5\text{ mm}$, $R_L = 1\,\Omega$) ; 100BASE-T1 (left) and CAN FD (right)

Another possible configuration is a coupling which does not occur over the entire length of the TWP. Therefore, the length of transmission line is varied, whereas the coupling length l_W is constant 0.5 m. That means, the length of TWP between the transceivers is $l_{TWP} = l_U + l_W$, with l_U being the uncoupled wire length. The impact of uncoupled TWP length on transfer function is shown in Fig. 13. The transfer function only changes slightly with different TWP length for 100BASE-T1 setup. There are only differences for frequencies greater 50 MHz. Depending on wire length the transfer function can decrease and a critical coupling in frequency range of 66⅔ MHz is possible. On the other hand, there are more differences in CAN FD network for different length of TWP.

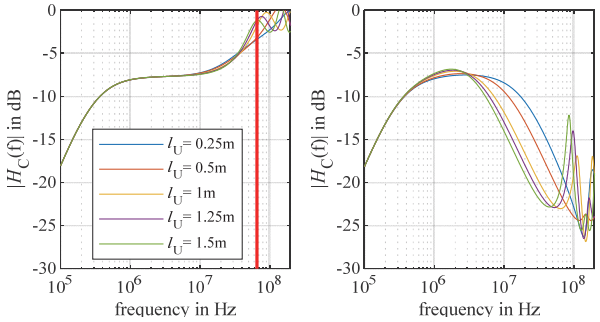

Fig. 13. Transfer function for varying length of uncoupled TWP l_U with constant coupling length ($l_w = 0.5\text{ m}$, $R_L = 1\,\Omega$, $d_W = 1.5\text{ mm}$); 100BASE-T1 (left) and CAN FD (right)

It has been shown, that at some frequencies the sensitivity of the communication system against disturbances is very high. Strong coupling can be found for both systems at these frequencies.

IV. Investigations on Mode-Conversion

In this section, the mode conversions within the bus systems are evaluated. Measurements and simulations are performed to analyze mode conversion.

A. Theoretical considerations

At first, some theoretical aspects of the mode conversion are discussed. In a communication system a common to differential mode conversion can be caused by imbalances in the TWP or asymmetries within termination networks.
Within two coupled wires mode conversion can be caused by imbalances of the structure due to different radii or heights over ground plane. In a TWP the radii are the same, but the heights over ground change cyclically along the wire length with the assumption of an ideal bifilar helix. In an idealized consideration, the two wires of the TWP rotate on a circle around a common center per length of one twist s. If an infinitesimal section of the TWP is considered, a configuration of parallel wires over ground can be assumed, as shown in the cross section in Fig. 14. The following calculation is performed for the per unit length parameter inductance matrix, but can performed analogously for the capacitance matrix (cf. [14]). In (2) the general inductance matrix and similarity transformation matrices are shown to compute the parameters in terms of CM and DM quantities.

$$\boldsymbol{L'} = \begin{bmatrix} l_{11} & l_{12} \\ l_{21} & l_{22} \end{bmatrix},\ \boldsymbol{T}_V = \begin{bmatrix} 1 & 1/2 \\ 1 & -1/2 \end{bmatrix},\ \boldsymbol{T}_I = \begin{bmatrix} 1/2 & 1 \\ 1/2 & -1 \end{bmatrix} \tag{2}$$

Using the transformation matrices, the modal per unit length parameters can be calculated as shown in (3). In case of a well-balanced geometry, same heights and same radii, the out-diagonal entries are null. In an imbalanced setup these parameters are responsible for mode conversion.

$$\boldsymbol{L'}_M = \boldsymbol{T}_V^{-1} \cdot \boldsymbol{L'} \cdot \boldsymbol{T}_I = \begin{bmatrix} l_{CM} & \Delta l \\ \Delta l & l_{DM} \end{bmatrix} \tag{3}$$

In case of a configuration of parallel wires over ground $\boldsymbol{L'}$ and $\boldsymbol{C'}$ matrices can be calculated based on the geometry parameters presented in [15]. These are inserted into equation (3) which leads to an expression of Δl.

$$\Delta l = \frac{l_{11} - l_{22}}{2} = \frac{\mu}{4\pi} \ln\left(\frac{h_1}{h_2}\right) = \frac{\mu}{4\pi} \ln\left(\frac{h - \frac{d_{TWP}}{2} \cdot \sin\left(2\pi \frac{z}{s}\right)}{h + \frac{d_{TWP}}{2} \cdot \sin\left(2\pi \frac{z}{s}\right)}\right) \tag{4}$$

The calculation of Δc and Δl with the parameters introduced in Fig. 6 are shown in Fig. 14 (right) for one twist length. These parameters are periodic with twist length s. Over the length of the whole wire the effects of changing parameters cancel each other assuming an ideal twisted wire. In a real system, nonuniformity is possible (cf. [16]) and especially the end of the TWP has to be considered where incomplete twists can occur or even twisting is not possible e.g. within plugs or on PCBs. Besides the mode conversions an asymmetric coupling is possible within imbalanced parts of a TWP. This was investigated in detail in a previous work [17].

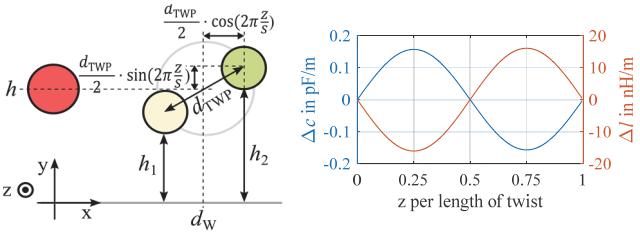

Fig. 14. Geometry of TWP (left) and calculation of Δc and Δl for investigated configuration (right)

In this paper, the focus is put on asymmetries within termination networks. Calculation results of Δc and Δl parameters are rather small and therefore asymmetries in TWP are dominated by those in termination networks. The resulting DM voltage caused by asymmetric termination network are investigated in the following.

B. Measurement based investigation on mode conversion

Asymmetries of the termination resistors in a CAN FD communication network are examined exemplarily, to figure out the influences on mode conversion and especially differential mode voltage at transceiver input.
The measurement setup is shown in Fig. 15. The coupling structure is built analogue to Fig. 1 with a single wire and a

TWP of the communication system in parallel. The disturbing circuit consists of a trapezoidal pulse source and is terminated with 50 Ω. The coupling length is 1.6 m and the distance between the wires is 1 cm. The communication nodes are built up with evaluation boards with removed ICs to measure the influence of the termination network only. The voltages are measured behind the termination network with active voltage probes and an oscilloscope. The corresponding simulation setup is also shown in Fig. 15.

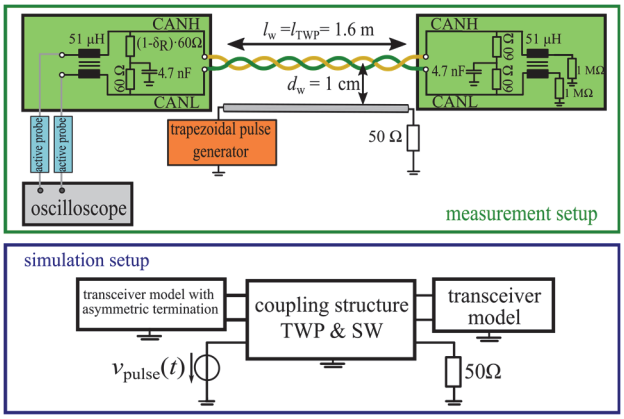

Fig. 15. Measurement setup to investigate asymmetries within termination network and corresponding simulation setup

1) Measurement results

The results of the measurements are shown in Fig. 16. Three different pulses with maximum amplitude voltage V_S and rise time of 5 ns are used as well as two different deviations of termination resistors δ_R. The maximum differential voltage increases with increasing amplitude V_S and increasing asymmetry. The measurement results are compared to simulations. Using these exemplary asymmetric coupling structures, it is shown that the DM voltages on the TWP depending on trapezoidal disturbing pulse are properly modeled with the introduced simulation setup. The maximum differential mode voltage $|V_{DM,max}|$ is also plotted in the figure, which is evaluated in the following investigations (IV.C).

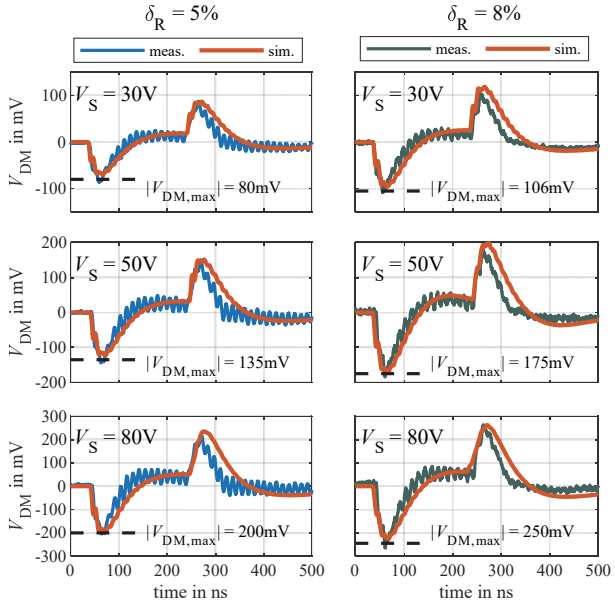

Fig. 16. Measurement results for different maximum amplitudes V_S and deviations of termination resistor

C. Simulation based investigation on mode conversion

In order to investigate asymmetries within termination networks in detail simulations are performed. These asymmetries can occur in termination resistors and CMCs. For these investigations, the models of the termination networks are adapted as shown in Fig. 17. The green marked termination resistors have a deviation δ_R to their nominal values from 0 to 10 %. Besides the termination resistors asymmetries can occur in the common mode choke. In [18] the asymmetry of common mode chokes of CAN FD networks is investigated. The root cause of asymmetry in CMCs is the stray inductance, which is introduced with ΔL in the equivalent circuits. According to [18] CMCs can show asymmetries from 10 nH to 300 nH.

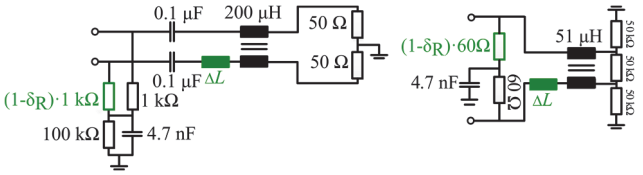

Fig. 17. Adapted model approaches for investigation on mode conversion of 100BASE-T1 (left) and CAN FD (right)

A time domain simulation is performed to determine the maximum DM voltage. The simulation setup is built up according to Fig. 1 with the following parameters: $R_L = 1\ \Omega$, $l_{TWP} = l_W = 1$ m, $d_W = 1.5$ mm, $R_S = 0.1\ \Omega$. In contrast to the measurement shown, the simulations use a coupling configuration close to the worst-case according to the results of chapter III.C. The component values are varied at just one of the two termination networks in the point-to-point communication setup. A trapezoidal signal is assumed in the generating circuit with maximum amplitude V_S. and rise time of 3 ns.

1) 100BASE-T1 results

The common mode termination is an important part of the physical layer of 100BASE-T1 transceiver [3]. The green marked resistor in Fig. 17 has the nominal value of 1 kΩ. The results of the maximum DM voltage $|V_{DM,max}|$ depending on deviation δ_R are depicted in Fig. 18 for three different maximum voltages of the switching pulse. The critical value of differential mode disturbance according to [19] is 0.6 V and is also marked in the figure.

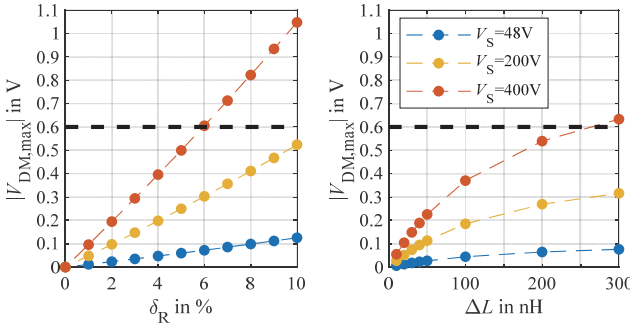

Fig. 18. Maximum differential mode voltage depending on asymmetry within common mode termination (left) and common mode choke (right) of 100BASE-T1 termination network

The results show an increasing DM disturbance voltage with increasing deviation of termination resistor. In case of maximum amplitude V_S of 48 V and 200 V the disturbance voltage does not reach the critical value. Only in case of pulse

voltage amplitude of 400 V the critical value can be exceeded. In the evaluation, it must be considered that only one parameter of a termination is varied in the simulation. In a real setup, deviations of all components can lead to a stronger asymmetry of the setup. The maximum DM voltage depending on ΔL are also shown in Fig. 18. In a 100BASE-T1 setup, the differential mode disturbance only reaches the critical value of 0.6 V for a voltage of 400 V and a large asymmetry.

2) CAN FD results

In a CAN FD setup the impact of asymmetries within termination impedance are also analyzed. In Fig. 19 the resulting DM voltage is shown depending on the deviations of a 60 Ω termination resistor and the stray inductance of CMC (cf. Fig. 17). The critical value of differential mode voltage is assumed to be 1.1 V [19]. This value is reached for 200 V and 400 V in the considered range of deviation δ_R. However, even for a voltage of 48 V the critical differential mode voltage is nearly reached. The asymmetry of the CMC is also investigated with the approach described for 100BASE-T1. The maximum differential mode voltage is determined depending on stray inductance ΔL. It can be seen, that the asymmetry of the choke does not result in a critical differential mode disturbance within a CAN FD network. The differential mode disturbance voltage is much lower than in the 100BASE-T1 setup.

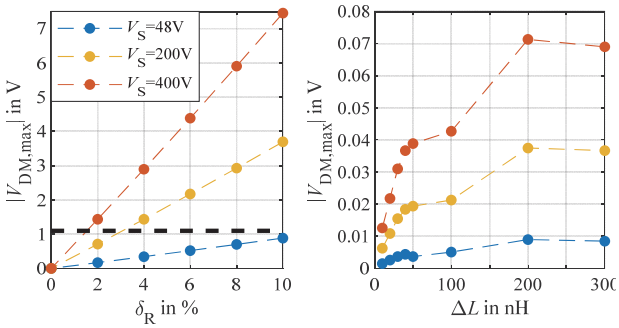

Fig. 19. Maximum differential mode voltage depending on asymmetry within termination resistors (left) and common mode choke (right) of CAN FD termination network

The investigations figured out, the potential interferences caused by asymmetry in the physical layer. Especially asymmetry of the termination resistors can cause critical mode conversion in both communication systems. The asymmetry of CMC has a greater impact on 100BASE-T1. However, within a 48 V system the investigated coupling could not lead to critical disturbances, even within an asymmetric setup.

V. Conclusion

In this paper, wire coupling configurations and their impact on the communication systems CAN FD and 100BASE-T1 is evaluated. In coupling configurations, mode conversion in particular leads to a large interference potential because of the differential signaling of the systems. The presented simulation models are used to quantify the wire coupling and mode conversion. The transfer functions describing wire coupling are determined and critical configurations are analyzed. At some frequencies a strong coupling can reached, also in frequency ranges used for transmission. Therefore, critical common mode disturbing voltages can arise on the communication wire. To ensure robust communication a high symmetry must be achieved to avoid differential mode disturbances, which was been quantified by measurements and simulative investigations of asymmetries in the termination network.

Acknowledgment

The work in this paper was funded by the German Federal Ministry of Education and Research as part of the project RobKom (Robuste Kommunikation in autonomen Elektrofahrzeugen) with reference number 16EMO0380. The responsibility for this publication is held by the authors only.

References

[1] *CAN with Flexible Data-Rate Specification,* Version 1.0, Robert Bosch GmbH, 2011

[2] IEEE Standard for Ethernet: Amendment 1: Physical Layer Specifications and Management Parameters for 100 Mb/s Operation over a Single Balanced Twisted Pair Cable (100BASE-T1), IEEE Computer Society, 2015

[3] K. Matheus und T. Königseder: *Automotive Ethernet*, Cambridge University Press, 2014

[4] S. Jeschke, A. H. Razavi, J. Loos and J. Baerenfaenger, "Impact of HV Battery Cables' Emissions on the Signal Integrity of 2-Wire Ethernet Communication in Automotive Application," *EMC EUROPE*, Barcelona, Spain, 2019

[5] S. Jeschke, J. Loos and M. Kleinen, "Impact of Highly Efficient Power Electronics on the EMC in Electric Vehicles With Autonomous Driving Functions," *AmE 2020 - Automotive meets Electronics; 11th GMM-Symposium*, Dortmund, Germany, 2020

[6] H. Chen, T. Wang, "Estimation of Common-Mode Current Coupled to the Communication Cable in a Motor Drive System," *IEEE Trans. Electromagn. compat.*, vol. 60, no. 6, 2018

[7] M. Fontana, F. Canavero and R. Perraud „Intergrated Circuit Modeling for Noise Susceptibility Prediction in Communication Networks", *IEEE Trans. Electromagn. Compat.*, vol. 57, no. 3, 2015

[8] User Manual DSO-8/TSON-8 Demoboard-Z8F62791012, Rev. 1.0, infineon, 2018

[9] S. Mortazavi, D. Schleicher and F. Gerfers, "Modeling and Verification of Automotive Multi-Gig Ethernet Communication up to 2.5 Gbps and the Corresponding EMC Analysis," *IEEE Symp. on Electromagn. Compat., Signal Integrity and Power Integrity,* Long Beach, CA, 2018

[10] User's Guide DP83TC811EVM, Texas Instruments, 2017

[11] S. Mortazavi, D. Schleicher and F. Gerfers, "Characterization of common-mode choke for automotive ethernet networks enabling 100 Mbit/s," *EMC EUROPE*, Angers, 2017

[12] S. Greedy, C. Smartt, M. J. Basford and D. W. P. Thomas, "Open source cable models for EMI simulations," *IEEE Trans. Electromagn. Compat.*, vol. 7, no. 3, pp. 69-81, 2018

[13] C. Smart, D. Thomas, S. Greedy et al., SACAMOS: Theory Manual V1.2, University of Nottigham, 2018

[14] F. Grassi, Y. Yang, X. Wu, et al., "On Mode Conversion in Geometrically Unbalanced Differential Lines and Its Analogy With Crosstalk," *IEEE Trans. Electromagn. Compat.*, vol. 57, no. 2, 2015

[15] F. M. Tesche, M. V. Ianoz and T. Karlsson, *EMC Analysis Methods and computational Models*, John Wiley & Sons, New York, 1997

[16] G. Spadacini, F. Grassi and S. A. Pignari, "On the combined effect of random nonuniformity and deformation of twisting on the radiated immunity of twisted-wire pairs," *2013 IEEE Intern. Symp. on Electromagn. Compat.*, Denver, 2013

[17] C. Austermann., S. Frei, "Impact of WBG-Semiconductors on Automotive Communication Networks", *EMC EUROPE*, Barcelona, Spain, 2019

[18] S. Miropolsky and M. Roebl, "Uncertainty of CAN RF Emission Test Results due to Common Mode Choke Asymmetry", *EMC EUROPE*, Barcelona, Spain, 2019

[19] C. Austermann., S. Frei, "Störfestigkeit von Automotive Ethernet Kommunikationssystemen", *EMV Köln*, Germany, 2020